Available online at www.sciencedirect.com
ScienceDirect
Journal of Sound and Vibration 297 (2006) 563–577
JOURNAL OF SOUND AND VIBRATION
www.elsevier.com/locate/jsvi

# Cylinder wake influence on the tonal noise and aerodynamic characteristics of a NACA0018 airfoil

Y. Takagi, N. Fujisawa*, T. Nakano, A. Nashimoto

*Department of Mechanical Engineering, Niigata University, 8050 Ikarashi-2, Niigata, 950-2181 Japan*

Received 28 May 2004; received in revised form 21 December 2005; accepted 10 April 2006
Available online 30 June 2006

**Abstract**

The influence of cylinder wake on discrete tonal noise and aerodynamic characteristics of a NACA0018 airfoil is studied experimentally in a uniform flow at a moderate Reynolds number. The experiments are carried out by measuring sound pressure levels and spectrum, separation and the reattachment points, pressure distribution, fluid forces, mean-flow and turbulence characteristics around the airfoil with and without the cylinder wake. Present results indicate that the tonal noise from the airfoil is suppressed by the influence of the cylinder wake and the aerodynamic characteristics are improved in comparison with the case without the cylinder wake. These are mainly due to the separation control of boundary layers over the airfoil caused by the wake-induced transition, which is observed by surface flow visualization with liquid- crystal coating. The PIV measurements of the flow field around the airfoil confirm that highly turbulent velocity fluctuation of the cylinder wake induces the transition of the boundary layers and produces an attached boundary layer over the airfoil. Then, the vortex shedding phenomenon near the trailing edge of pressure surface is removed by the influence of the wake and results in the suppression of tonal noise.


## 1. Introduction

It is well known that discrete tonal noise is generated from an airfoil, which is inclined at a small attack angle to the free stream at moderate Reynolds numbers. Such noise is commonly heard from various types of turbo-machineries, such as wind turbine, aircraft, compressor, fan and so on. Therefore, various research has been conducted on this subject to understand the mechanism of tonal noise and its control for the purpose of noise reduction.

Most previous studies are concerned with the experimental and theoretical analysis of tonal noise generated from 2D airfoil located in a uniform flow [1–4]. Some of them studied the practical problem of tonal-noise characteristics from turbo-machineries [5,6]. These investigations commonly suggest that the tonal noise is caused by the growth of Tollmien–Schlichting type instability of the laminar boundary layer over an airfoil in conjunction with the self-excited feedback mechanism of acoustic field between the trailing edge and the unstable shear layer. However, the validity of this mechanism is proved later in more recent studies [7,8],

*Corresponding author. Tel./fax: +81 25 262 6726.
*E-mail address:* fujisawa@eng.niigata-u.ac.jp (N. Fujisawa).

0022-460X/$ - see front matter © 2006 Elsevier Ltd. All rights reserved.
doi:10.1016/j.jsv.2006.04.012

which find that tonal noise is determined by the velocity profiles of an unstable separated shear layer over the pressure surface of NACA0012 airfoil. Later, tonal noise mechanism of NACA0018 airfoil is studied using the flow-field measurement around the airfoil by particle image velocimetry (PIV) [9,10]. These results also indicate that the generation of tonal noise is associated with laminar separation and the periodic formation of vortices on the pressure surface near the trailing edge of the airfoil, which results in the vortex shedding downstream.

In most turbo-machineries, the flow around the airfoil is influenced by the wake originating from the preceding airfoil. Therefore, it is very important to study the influence of the wake on tonal noise characteristics of the airfoil. Although the aerodynamic characteristics under the influence of the preceding wake have been studied in relation to the laminar-turbulent transition of the boundary layer over airfoil [11–14], little is known about the noise characteristics, which are very important in practical applications. It is expected that the boundary layer over the airfoil becomes turbulent through the transition process by the interaction between the wake and the boundary layer. Then, the tonal noise characteristics are expected to vary by the influence of the upstream wake.

The purpose of the present paper is to study the influence of the wake on the characteristics of tonal noise and aerodynamic characteristics of a NACA0018 airfoil in uniform flow. The surface flow is visualized by liquid-crystal coating to detect the change of flow separation and reattachment points. Further, unsteady flow field around the airfoil is measured by PIV, which allows for the evaluation of mean flow and turbulence characteristics and the flow structure near the trailing edge of the airfoil.

## 2. Experimental apparatus and procedures

### 2.1. Experimental setup

The experiments are carried out using an acoustic wind tunnel [9]. The contraction ratio of the nozzle is 10, the total number of grids is six and the two honeycombs are located inside the wind tunnel. The dominant frequency of the blower noise (580 Hz at $U_0 = 30$ m/s) is reduced by a reactive-type silencer located downstream to the blower and the flow noise is reduced by a splitter-type silencer in the plenum chamber and a sound absorber material of 50 mm thickness inside the wind tunnel. The test section is a square cross-sectional area 190 mm × 190 mm and 500 mm long. The top and bottom surfaces are made of glass-wool material of 25 mm thickness and acrylic-resin material for the support to minimize acoustic resonance. The sidewalls of the test section are made transparent using acrylic resin for flow visualization purposes. The velocity distribution of free stream in the test section is uniform within 1% and the streamwise turbulence intensity is about 1% of the free-stream velocity, which are measured by hot-wire anemometry at free-stream velocity $U_0 = 30$ m/s.

The 2D model of a symmetrical airfoil NACA 0018 is placed at the mid position of the test section. The schematic illustration of the airfoil is shown in Fig. 1(a). Streamwise and normal coordinates are defined by $x$ and $y$, respectively, which originate from the airfoil axis, while $X$ and $Y$ are used for the chordwise and normal coordinates relative to the airfoil. The axis of rotation is located at $0.3C$ ( = 24 mm) from the leading edge of the airfoil, where the thickness of the airfoil reaches its maximum. The airfoil is symmetrical to the centerline and has a chord length of $C = 80$ mm and a spanwise length of 190 mm. The airfoil is made of acrylic resin for aerodynamic noise and fluid force measurements and also for flow visualization studies. However, the pressure measurements on the airfoil surface are carried out using an airfoil made of stainless steel due to the difficulty in machining the complex structure of pressure piping in the acrylic resin. The angle of attack $\alpha$ of the airfoil can be varied by rotating the airfoil about the axis.

In order to study the influence of wake on the tonal noise and aerodynamic characteristics of the airfoil, a circular cylinder is placed upstream from the airfoil. The cylinder is supported horizontally on both sidewalls of the wind tunnel and the position of the cylinder is varied stepwise at every 10 mm in horizontal direction $x_c = -160$ to $-40$ mm and in vertical direction $y_c = -50$ to 50 mm using a ladder-like structure on both sides of the cylinder. Here, $x_c$ and $y_c$ are the streamwise and vertical coordinates of the cylinder, respectively, with respect to the airfoil axis. Note that the diameter of the cylinder is set to 2.5 mm because it generates vortices at similar frequency to that of the airfoil.

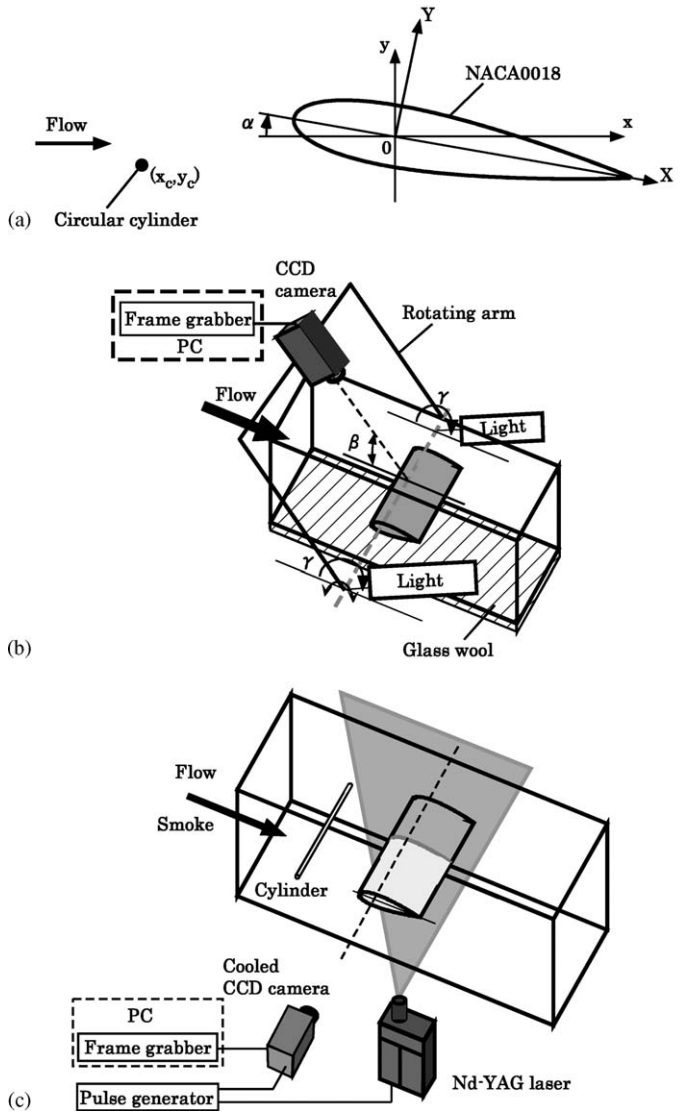


Fig. 1. Experimental apparatus: (a) Schematic illustration of flow field, (b) surface-flow visualization and (c) PIV measurement.

The free-stream velocity in the test section is set to $U_0 = 30\,\mathrm{m/s}$ in the present experiment, which corresponds to the Reynolds number $Re(= U_0 C/\nu) = 1.6 \times 10^5$, where ν is the kinematic viscosity of working fluid air.

### 2.2. Noise measurement

The sound pressure level and the spectrum of aerodynamic noise are measured by a condenser microphone placed below the glass-wool material of the bottom surface and at the airfoil axis. The microphone has a flat frequency response from 20 to 8000 Hz.The output voltage is digitized by A-D converter and the noise spectrum is calculated by FFT analysis in the computer. Accuracy of noise measurement is estimated as 1.2 dB at 95% coverage, which comes from calibration error of the microphone 1 dB and the random error due to the fluctuation of experimental data 0.3 dB.

### 2.3. Measurement of aerodynamic characteristics

The pressure distribution on the airfoil surface and the drag and lift forces are measured to understand the aerodynamic characteristics of the airfoil. Ten pressure holes of 0.8 mm in diameter are distributed on one side of the airfoil. The pressure on the airfoil surface is detected by a strain-gauge-type pressure transducer placed outside the test section, which is connected by the stainless-steel tubes of 1.8 mm diameter. Note that the pressure holes are distributed along the airfoil surface inclining at small angle to streamwise direction to minimize the influence of disturbances produced by the pressure holes upstream. The output signal from the pressure transducer is digitized by A-D converter and the time-averaging procedure is carried out in the computer. Accuracy of pressure measurement is estimated as 0.04 in pressure coefficient $C_p(=2(p-p_0)/\rho U^2)$ at 95% coverage, which comes from the linearity and the zero drift of the transducer 3% and the random error due to the fluctuation of experimental data 1% ($p$; pressure; $p_0$; reference pressure; $U_0$; free stream velocity; $\rho$; density of fluid).

The fluid forces on the airfoil are detected by a three-component strain-gauge-type force balance meter. The output signal is processed in a computer to evaluate the drag and lift forces on the airfoil. Note that the airfoil is placed vertically in the present measurement to minimize the influence of airfoil weight. The uncertainty of fluid force measurement is estimated as 0.05 in drag coefficient $C_d(=2F_x/\rho U^2 C)$ and lift coefficient $C_l(=2F_y/\rho U^2 C)$ at 95% coverage ($F_x$, streamwise fluid force of unit length, $F_y$, normal fluid force of unit length). This uncertainty comes from the linearity, zero drift and the calibration error of the force balance meter 5% and the random error due to the fluctuation of experimental data 1%.

### 2.4. Surface-flow visualization by liquid-crystal coating

The liquid crystal used in the present experiment is a mixture of cholesteric and chiral-nematic liquid crystal (BCN/195 Hallcrest), which is insensitive to temperature changes from 273 to 333 K. The liquid crystal mixed with petroleum ether is sprayed on the airfoil surface, which is painted black to enhance the color change of liquid crystal. The petroleum ether evaporates quickly after being sprayed and a thin-film coating of liquid crystal remains on the test surface. The thickness of the liquid crystal coating is estimated as 5 μm in the present experiment. Illumination is provided by two fluorescent lights and the color change of the liquid-crystal coating is observed by a color CCD camera ($768 \times 494$pixels with 8 bits for RGB, 30 frames/s). They are placed around the test section as shown in Fig. 1(b). The angles of observation $\beta = 60^\circ$ and illumination $\gamma = 150^\circ$ in the present experiment are determined from the most sensitive angles to the shear-stress changes [15–18]. Note that such illumination and observation angles against the airfoil chord are kept constant during the present experiment, which is realized by the rotation mechanism of observation and illumination system about the airfoil axis. Note that two lights are positioned at certain slanted angles from both sides of the airfoil to minimize the halation of the light on the airfoil surface.

The visualized images are converted into $HSI$ color format from RGB and $\Delta H$ is evaluated from the visualized images with and without airflow, where $H$, hue; $S$, saturation and $I$, intensity of color. Then, the separation and reattachment points over the airfoil surface are determined by the criteria that $\Delta H$ approaches zero [10]. The uncertainty of separation and reattachment points measurement $X/C$ is estimated as 0.02 at 95% coverage, which comes from the random error due to the fluctuation of experimental data.

### 2.5. PIV measurement of velocity field

The instantaneous velocity field around the airfoil is measured by PIV system shown in Fig. 1(c). It consists of a pair of Nd:YAG lasers, a high-resolution CCD camera and a pulse generator. A light sheet illumination is provided from the Nd:YAG lasers to visualize the 2D vertical cross-section of the airfoil at mid-span of the test section [9,19]. The lasers emit 532 nm wavelength pulse light with an energy of 50 mJ per pulse. The thickness of the light sheet is about 1 mm.Observation is made by a monochrome digital CCD camera having a spatial resolution of $1280 \times 1024$ pixels with 12 bits in gray level, which is operated in synchronous with the pulse signal from the pulse generator and the lasers. We selected 12 bit camera for higher intensity resolution of the low intensity light scattering from smoke particles of about 1 μm in diameter. The particle images are

captured at lowest 8 bits in the 12 bit image, so that the PIV analysis is carried out using an image information of 8 bits. The frame rate of the CCD camera is 4 frame/s and the time interval between the lasers is set to 3 μs. The captured images are stored in a frame memory in a computer through the frame grabber. Note that the telecentric lens ($F = 2.8$) is used in the present experiment to minimize the viewing angle effect.

The instantaneous velocity vectors are obtained by analyzing a pair of smoke images using the gray-level difference method for cross-correlation calculation between the sequential two images [20]. The interrogation window size is set to $31 \times 31$ pixels and the candidate region is searched for in the area $21 \times 21$ pixels to minimize erroneous velocity vectors with a reasonable spatial resolution in the analysis. The target images are taken in the area of 35 mm × 30 mm, so that the spatial resolution of the image is 0.03 mm/pixel. The interrogation window is overlapped by 50% to satisfy the Nyquist sampling criterion. The sub-pixel interpolation with Gaussian-peak-fitting is incorporated into the analysis to improve the accuracy of velocity measurement. The statistical properties of the mean flow and turbulence characteristics are obtained from 160 instantaneous velocity distributions. The accuracy of velocity measurement is found to be 5.2% of the free-stream velocity at 95% coverage, which comes from the RMS error in PIV analysis 2.6% derived from the artificial image analysis [21] (which corresponds to sub-pixel accuracy 0.09 pixel divided by the mean displacement of tracer particles in the image 3.5 pixel).

## 3. Results and discussions

### 3.1. Noise characteristics

Fig. 2 shows the noise level of the aerodynamic sound from the airfoil at various positions of the circular cylinder ($x_c$, $y_c$), where $x_c/C$ ranges from $-0.5$ to $-2$ and $y_c/C$ from $-0.625$ to 0.625 in the present experiment. The angle of attack of the airfoil is set to $\alpha = 6^\circ$, which corresponds to the condition of largest tonal noise [9]. The results indicate that the sound pressure level is reduced when the circular cylinder is placed on the pressure side of the airfoil ($y_c/C = 0$ to $-0.25$) for all the streamwise positions $x_c/C$ in the present experiment. It is expected that the flow over the pressure side of the airfoil is very influential on the generation of tonal noise from the airfoil.

Fig. 3 shows the variations of the sound pressure level with the change of attack angle of the airfoil with and without cylinder wake. Note that the measurement with the cylinder wake is carried out by placing the circular cylinder at a position ($x_c/C = -1$ and $y_c/C = -0.125$) upstream from the airfoil, where maximum noise reduction is found in Fig. 2. The result without the cylinder wake shows a clear indication of tonal noise at attack angles $\alpha = 3$–$6^\circ$. Such tonal noise is greatly weakened by the influence of the cylinder wake and the resulted sound pressure level is even lower than that of the zero attack angle. Maximum noise reduction is found to be at about 20dB, which is observed at $\alpha = 6^\circ$. The sound pressure level with the cylinder wake increases slightly with further increase in attack angles. This corresponds to the growth of separating region on the airfoil. Note that the sound pressure level with the cylinder wake is slightly larger than that without the

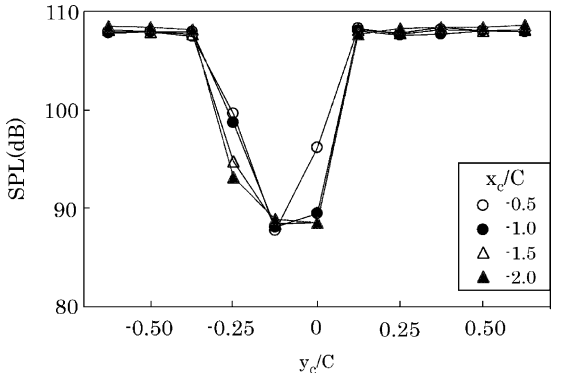


Fig. 2. Sound pressure level of aerodynamic noise at various positions of circular cylinder ($\alpha = 6^\circ$).

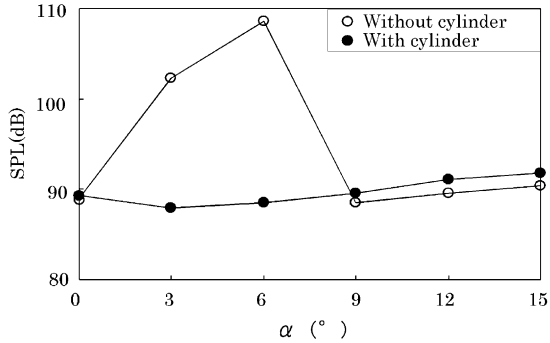


Fig. 3. Sound pressure level of aerodynamic noise at various angles of attack ($x_c/C = -2$, $y_c = -0.125$).

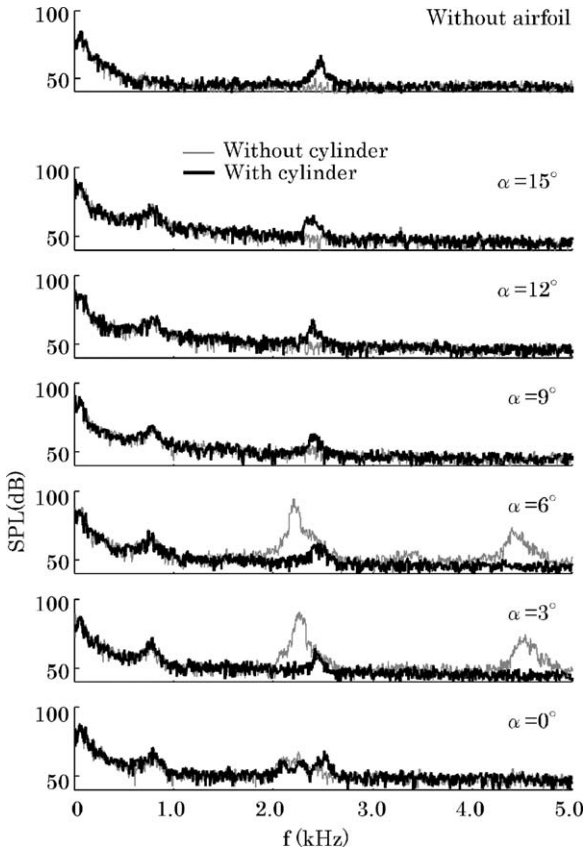


Fig. 4. Sound spectrum at various angles of attack α.

wake at attack angles larger than 9°, which is due to the vortex shedding noise from the circular cylinder as seen in the noise spectrum of the circular cylinder in Fig. 4. It is believed that such reduction in sound pressure level of 15–20 dB at $\alpha = 3$–6° is expected to be due to the modification of the flow around the airfoil by the wake-induced transition of boundary layer on the pressure surface. The mechanism will be discussed in the section of surface flow visualization.

Fig. 4 shows the noise spectrum with and without the cylinder wake at various attack angles. Note that the circular cylinder is placed at $x_c/C = -1$ and $y_c/C = -0.125$. The noise spectrum without the cylinder wake

indicates that high peaks are generated at small attack angles $\alpha = 3$–$6^\circ$, which have primary frequency $f = 2.3$ kHz and double frequency $f = 4.6$ kHz. The primary frequency of the noise corresponds to Strouhal number $St(= 2f\,\delta/U_0) = 0.15$ ($\delta$, thickness of laminar boundary layer at trailing edge of airfoil), which agrees with the experimental result [1] $St = 0.09$–$0.15$ within an experimental scattering of data. Therefore, the present result indicates the feature of tonal noise from a symmetrical airfoil. The tone-like spectrum is almost removed from the noise spectrum under the influence of the cylinder wake except for the small peak at frequency 2.5 kHz. This result suggests the reduction of noise level as observed in Fig. 3. The appearance of the small peak at 2.5 kHz in the spectrum is due to the generation of vortex shedding noise from the cylinder, because a similar peak is also found in the spectrum of cylinder flow without airfoil in Fig. 4. It is to be mentioned that the Strouhal number of the small peak is $St(= fd/U_0) = 0.21$, which agrees closely with a well-known value 0.2 in literature [22] ($d$, diameter of a circular cylinder). Note that the small peak around 800 Hz is due to the resonance of the sound field in the wind tunnel, because the small peak around 800 Hz is not observed in the background noise spectrum in Fig. 4.

### 3.2. Surface-flow visualization

The surface flow on the airfoil is visualized by using a shear-sensitive liquid-crystal coating at $\alpha = 6^\circ$. The typical examples of $\Delta H$ on the suction and pressure surfaces of the airfoil with and without the cylinder wake ($x_c/C = -1$ and $y_c/C = -0.125$) are shown in Figs. 5 and 6, respectively, where $\Delta H$ is relative hue values with respect to the hue values without flow. Each picture corresponds to $\Delta H$ without cylinder (a), $\Delta H$ with cylinder (b) and the variation of $\Delta H$ along the centerline of the airfoil (c). The variations of $\Delta H$ on the suction surface (Fig. 5) indicate that the flow separates at $X/C = -0.11$ and reattaches at $X/C = 0.13$ without the cylinder wake, which are obtained from the surface flow visualization by liquid-crystal coating. Note that the separation and reattachment points are obtained from the variation of relative hue, where $\Delta H$ approaches zero. Such surface flow characteristics are greatly modified by the influence of the cylinder wake, when the circular cylinder is placed at $x_c/C = -1$ and $y_c/C = -0.125$. It is seen that the separating region on the airfoil

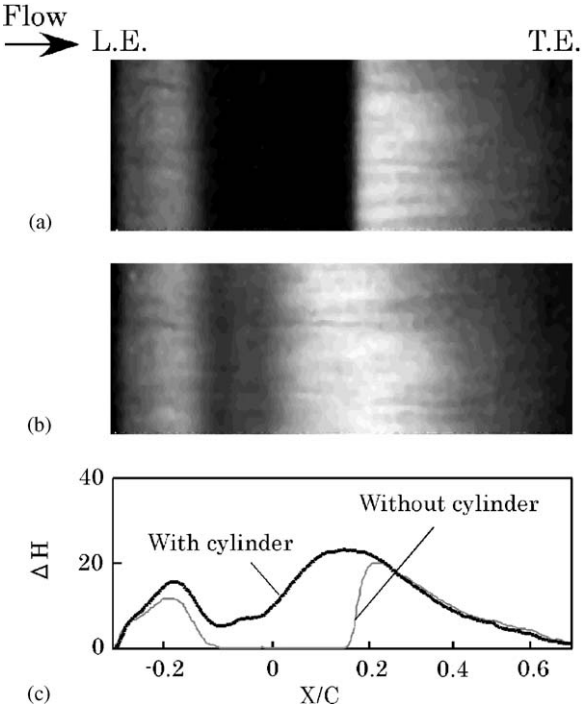


Fig. 5. Surface-flow visualization by liquid-crystal coating on suction surface: (a) without cylinder, (b) with cylinder and (c) chordwise variation of $\Delta H$.

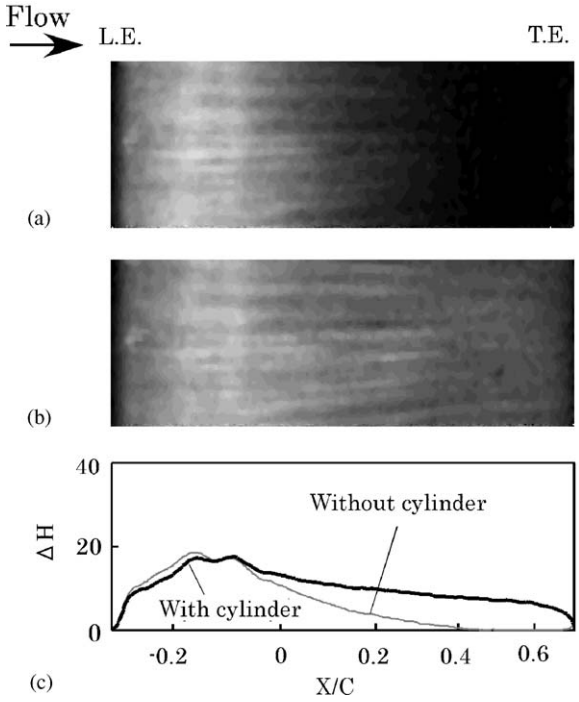


Fig. 6. Surface-flow visualization by liquid-crystal coating on pressure surface: (a) without cylinder; (b) with cylinder and (c) chordwise variation of $\Delta H$.

is almost removed under the influence of the cylinder wake, which is found by the positive $\Delta H$. This is expected to be due to the laminar-turbulent transition of the boundary layers on the suction surface of the airfoil. On the other hand, the distribution of $\Delta H$ on the pressure surface (Fig. 6) is influenced by the cylinder wake, too. The wake effect appears on the rear side of the airfoil, where $\Delta H$ with the cylinder wake becomes larger than that without the cylinder wake. This result corresponds to the downstream movement of the separation point from $X/C = 0.41$ to the trailing edge of airfoil under the influence of the cylinder wake.

Fig. 7 shows the contour map of separation and reattachment points of the boundary layers on the airfoil surfaces, which are obtained from many surface-flow visualizations using shear-sensitive liquid crystal coatings. The separation and reattachment points at $\alpha = 0^\circ$ without the cylinder wake are found on the mid-chord of the airfoil $X/C = 0.16$ and 0.49, respectively. They move upstream along the suction surface and downstream along the pressure surface with an increase in attack angle. Note that the separating region is created between the separation and reattachment points, which is shown by shaded area in Fig. 7. The separating region on the pressure surface is found to be longer than that on the suction surface, which is due to the gradual change of the surface flow pattern on the pressure surface as observed in Figs. 5 and 6. When the boundary layers on the airfoil are influenced by the cylinder wake ($x_c/C = -1$, $y_c/C = -0.125$), the flow separation on the airfoil is almost removed except for the small separating region on the suction surface, which is observed at a small attack angle less than 3°. This result indicates that the boundary layers on the airfoil at $\alpha = 6^\circ$ are fully attached to the airfoil surfaces due to the laminar-turbulent transition of boundary layers by the influence of the cylinder wake.

### 3.3. Aerodynamic characteristics

The pressure distribution on the airfoil surfaces with and without cylinder wake are measured to understand the change of aerodynamic performance by the influence of the cylinder wake ($x_c/C = -1$ and $y_c/C = -0.125$). The measured pressure coefficient $C_p$ along the airfoil surface is plotted against the distance $X/C$ at three typical angles of attack $\alpha = 0^\circ$, 6° and 15°, which is shown in Fig. 8.

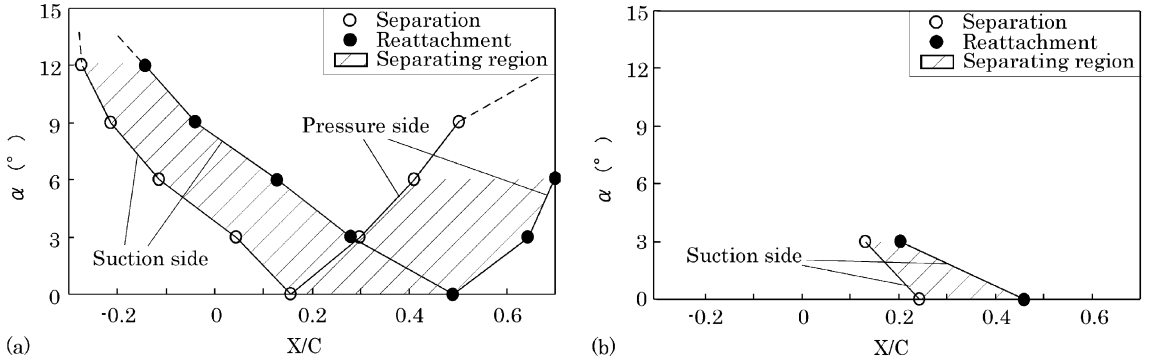


Fig. 7. Variation of separation and reattachment points along airfoil surface at various angles of attack: (a) without cylinder and (b) with cylinder.

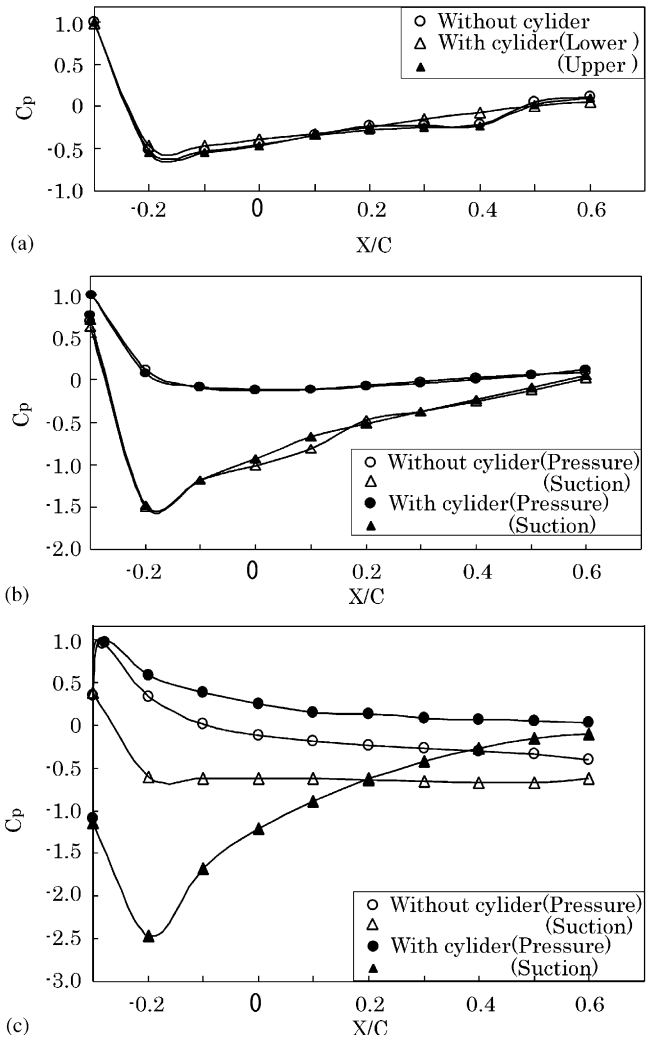


Fig. 8. Pressure distribution on airfoil surface: (a) $\alpha = 0^\circ$; (b) $\alpha = 6^\circ$ and (c) $\alpha = 15^\circ$.

The pressure distribution on the airfoil surface at $\alpha = 0^\circ$ without the cylinder wake collapses on a single curve due to the symmetrical configuration of the flow around the airfoil. When the circular cylinder is placed at $x_c/C = -1$ and $y_c/C = -0.125$, the pressure distribution becomes asymmetrical due to the off-axis displacement effect of the circular cylinder relative to the airfoil axis. The pressure distribution on the lower surface (cylinder side) is modified by the influence of the cylinder wake, while that on the upper surface of the airfoil agrees closely with the case without cylinder. Therefore, the pressure coefficient on the lower surface of the airfoil is slightly increased on the rear side of the airfoil in comparison with that on the upper surface. This is due to the removal of flow separation on the lower surface by the influence of cylinder wake.

When the attack angle increases to $\alpha = 6^\circ$, the pressure distribution becomes asymmetrical about the flow axis and the pressure on the suction surface decreases and that on the pressure surface increases. This modification of pressure distribution is consistent with the variation of separation and reattachment points as shown in Fig. 7. On the other hand, pressure distribution on the suction surface with cylinder wake reveals a small increase at the mid-chord of the airfoil in comparison with that without cylinder, which indicates an attached flow pattern on the suction surface due to the influence of the wake. Note that the increase in turbulence intensities and Reynolds stress are observed on the suction surface of the airfoil, which indicates the influence of the cylinder wake on the suction surface (see Figs. 12–14). The pressure distribution on the pressure surface with cylinder wake remains the same as that without cylinder wake, in spite of the difference in the separation region in the rear side of the airfoil (Fig. 7). Therefore, the change in flow separation on the pressure surface of airfoil by the influence of cylinder wake does not modify the pressure distribution on the pressure surface so much. This result may be related to the gradual change of surface flow pattern on the pressure surface with and without the cylinder wake as shown in Fig. 6.

With an increase in attack angle to $\alpha = 15^\circ$, the pressure distribution on the suction surface experiences a sudden increase near the leading edge of the airfoil without the cylinder wake. This result indicates that the flow on the suction surface separates near the leading edge of the airfoil and a recirculating region is formed over the whole area of the airfoil. The pressure distribution on the suction surface with cylinder decreases much more than that without the cylinder wake near the front side of the airfoil, which shows the attached flow by the influence of cylinder wake as observed in Fig. 7. It is expected that the boundary layer on the suction surface of the airfoil near the leading edge undergoes laminar-turbulent transition by influence of cylinder wake, which acts to remove the separating region and creates an attached flow over the airfoil at large attack angles. The pressure distributions on the pressure surface increases in the whole surface area, which indicates the presence of attached flow without separation.

Fig. 9 shows the drag and lift coefficients $C_d$, $C_l$ on the airfoil, which are plotted against the angles of attack $\alpha$. Each figure shows the results with and without cylinder wake. Note that the drag and lift coefficients evaluated from the pressure measurements are also plotted in this figure for comparative purposes. It is found that these results agree closely with each other within an experimental accuracy, suggesting the validity of the present measurement of pressures and fluid forces. The present results indicate that the drag force decreases and lift force increases at relatively large attack angles beyond $\alpha = 12^\circ$, which are due to the influence of

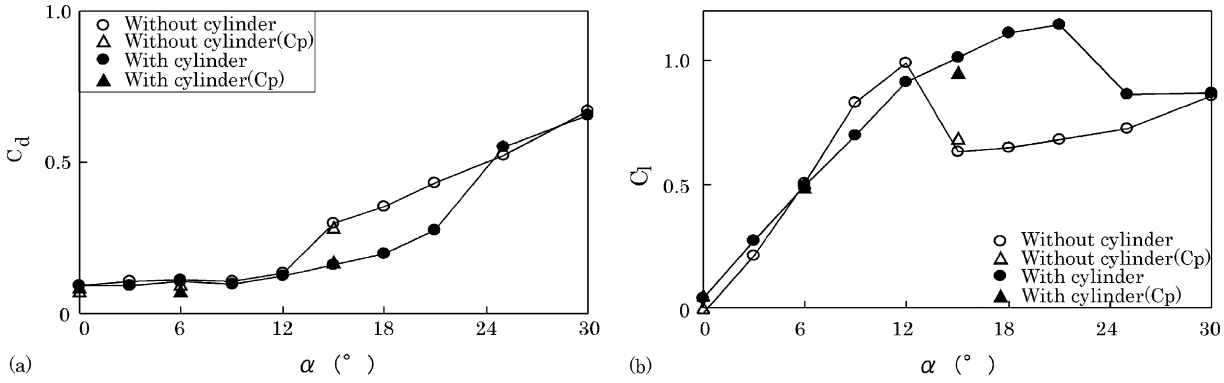


Fig. 9. Drag and lift coefficient of airfoil: (a) drag coefficient and (b) lift coefficient.

cylinder wake on the fluid forces. These results show an improvement in aerodynamic performance of the airfoil by the influence of cylinder wake except for the lift coefficient at $\alpha = 9$–$12^\circ$. However, the aerodynamic performance approaches the results without cylinder at attack angles larger than $25^\circ$. It is expected that the flow separates near the leading edge of the airfoil at such attack angles without reattachment and forms a large separating region downstream, which are considered to be insensitive to the cylinder wake.

### 3.4. Mean-flow characteristics

Fig. 10 shows the mean-velocity vectors and the contour of streamwise-velocity magnitude $u/U_0$ around the airfoil with and without the cylinder wake ($x_c/C = -1$ and $y_c/C = -0.125$), which are measured by PIV. The attack angle of the airfoil is set to $\alpha = 6^\circ$, where the largest tonal noise is observed in the present experiment. It also gives the points of flow separation and reattachment obtained from the surface-flow visualization by liquid-crystal coating. The mean-velocity distribution without cylinder indicates that the mean velocities on the suction surface are accelerated near the leading edge and recover downstream. The flow over the pressure surface decelerates near the front side due to the stagnation effect and accelerates slightly downstream. Although these velocity distribution features are well reproduced in the results with cylinder, quantitative differences can be seen in the flow over the pressure surface of the airfoil, which is due to the direct influence of cylinder wake on the velocity field. The velocity magnitude is reduced near the leading edge of the pressure surface by the influence of the cylinder wake. Except for this, the mean-velocity field with cylinder is similar to that without cylinder. Therefore, the modification of flow separation and reattachment of the boundary layer by influence of the cylinder wake seems to be limited to the near-wall region of the flow over the airfoil.

Fig. 11 shows the close-up view of instantaneous velocity vectors and the vorticity field with and without cylinder wake at attack angle $\alpha = 6^\circ$, where the vorticity $\xi$ is defined by $\zeta = C/U_0(\partial v/\partial x - \partial u/\partial y)$. It is found from the result without cylinder that the vortex structure is generated from the rear side of the pressure surface and sheds downstream, which results in a formation of periodic vortex street downstream from the airfoil. The vorticity magnitude is larger on the pressure surface than on the suction surface, which suggests the generation of tonal noise from the pressure surface near the trailing edge of airfoil. These features are consistent with the previous observation [9]. The spacing of the periodical structure in the wake is found to be $s/C = 0.12$–$0.14$ and the convection velocity of the vortices is about $0.8U_0$, so that the shedding frequency can be estimated as 2.1–2.5 kHz, which agrees with the tonal noise frequency 2.3 kHz in the present experiment. On the other

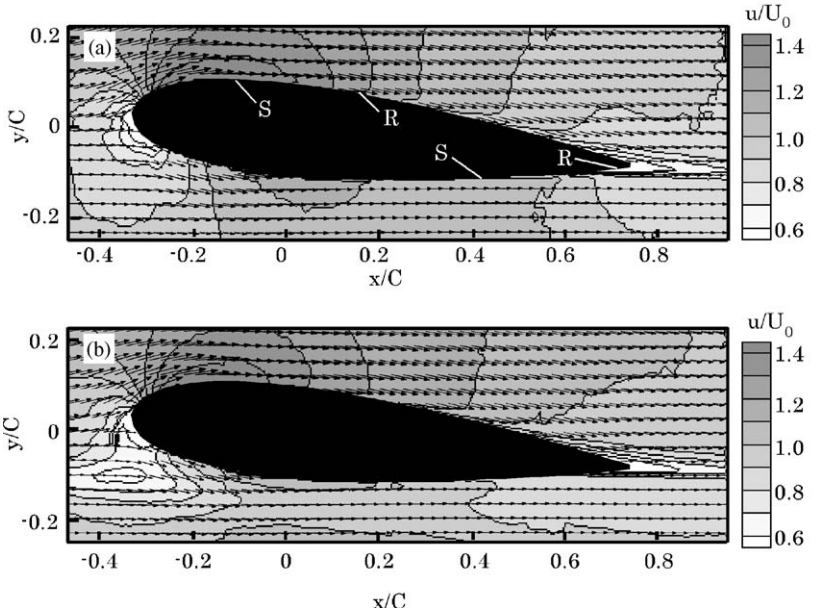


Fig. 10. Contour of mean velocity around airfoil at $\alpha = 6^\circ$ (R, reattachment; S, separation). (a) without cylinder and (b) with cylinder.

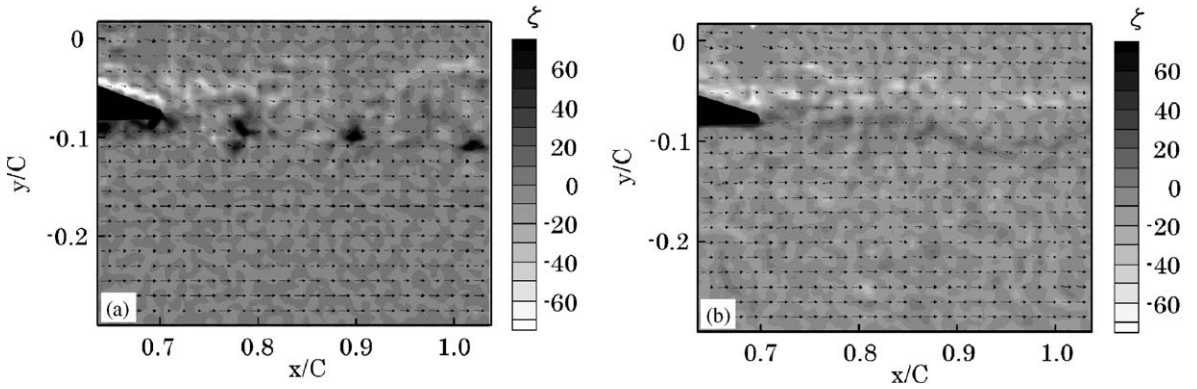


Fig. 11. Instantaneous velocity field in airfoil wake at $\alpha = 6^{\circ}$: (a) without cylinder and (b) with cylinder.

hand, the vorticity field under the influence of the cylinder wake indicates that the vorticity magnitude is reduced in the wake of the airfoil. This is due to the formation of the attached turbulent boundary layer on the pressure surface by the influence of the cylinder wake, which results in the removal of periodical vortex shedding in the wake of the airfoil.

### 3.5. Turbulence characteristics

Figs. 12 and 13 show the contours of streamwise $u_{\mathrm{rms}}/U_0$ and normal turbulence intensities $v_{\mathrm{rms}}/U_0$ around the airfoil, respectively, where the angle of attack is $\alpha = 6^{\circ}$. Each figure indicates results with and without the cylinder wake ($x_c/C = -1$ and $y_c/C = -0.125$). The positions of flow separation and reattachment are shown on the airfoil surface, which are obtained from the surface flow visualization by the shear-sensitive liquid crystal coating. The contours of streamwise and normal turbulence intensities without cylinder indicate that the highly turbulent region is generated around and downstream from the reattachment points on the airfoil surface. The highest turbulence intensities are observed downstream from the trailing edge of airfoil, where periodic vortex shedding is observed as shown in Fig. 11. On the other hand, the contours of streamwise and normal turbulence intensities are greatly modified by the influence of the cylinder wake. A large deviation is observed in the turbulence intensities over the pressure surface of the airfoil, which is due to the direct influence of the cylinder wake prevailing downstream. Due to the velocity fluctuations of the cylinder wake, the boundary layer on the pressure surface is forced to a turbulent state through the wake-induced transition process. Thus, the separation of the boundary layer on the pressure surface is removed under the influence of the cylinder wake and the turbulent boundary layer prevails over the pressure surface. The formation of the attached boundary layer on the rear side of the pressure surface contributes to the suppression of periodic vortex shedding from the trailing edge of the airfoil, which is due to the removal of instability in the laminar separating flow and the following reattachment of the flow near the trailing edge of the airfoil [10]. It is to be noted that the flow over the suction surface is also promoted to turbulent state by the influence of the cylinder wake, which results in the removal of separation on the suction surface except for with small attack angles as seen in Fig. 7.

Fig. 14 shows the contours of Reynolds stress $\overline{u'v'}/U_0^2$ around the airfoil with and without cylinder at attack angle $\alpha = 6^{\circ}$. The contour of Reynolds stress without cylinder shows that the large magnitude of Reynolds stress is observed in the rear side of airfoil and in the wake, which indicates the formation of periodic vortex shedding from the pressure surface of the airfoil. When the cylinder is placed upstream from the airfoil, the trace of the cylinder wake is found over the front side of the pressure surface, which is similar to the observation of turbulence intensities in Figs. 12 and 13. It is clearly seen that the high peak of Reynolds stress on the pressure surface near trailing edge of airfoil is removed and the magnitude of Reynolds stress in the wake of the airfoil is reduced in comparison with the result without cylinder. These results are associated with the removal of separation on the pressure surface and the following formation of attached flow near the

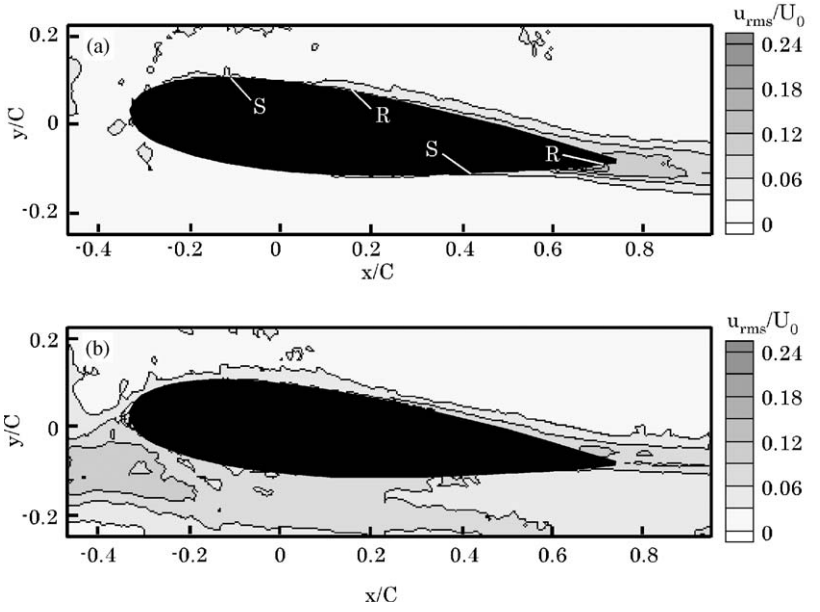


Fig. 12. Contour of streamwise turbulence intensity around airfoil at $\alpha = 6^\circ$ (R, reattachment; S, separation). (a) without cylinder and (b) with cylinder.

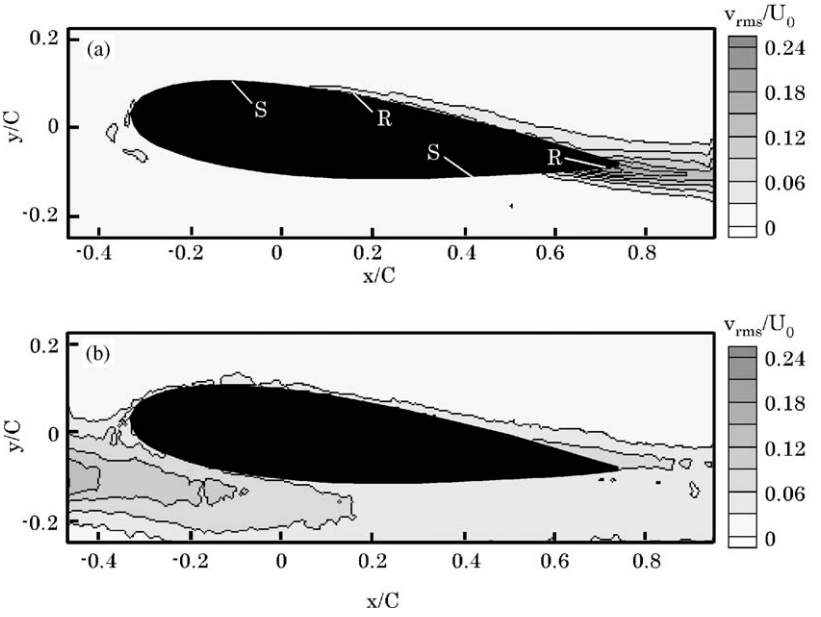


Fig. 13. Contour of normal turbulence intensity around airfoil at $\alpha = 6^\circ$ (R, reattachment; S, separation). (a) without cylinder and (b) with cylinder.

trailing edge of the airfoil, which are caused by the wake-induced transition of boundary layer on the pressure surface. Therefore, the present experimental results show that the tonal noise mechanism due to the instability of separating shear layer on the pressure surface is removed by the influence of cylinder wake and results in the suppression of tonal noise from the airfoil. It should be also mentioned that the change in noise is due primarily to the pressure surface boundary layer, while the change in lift and drag is due primarily to the suction surface boundary layer.

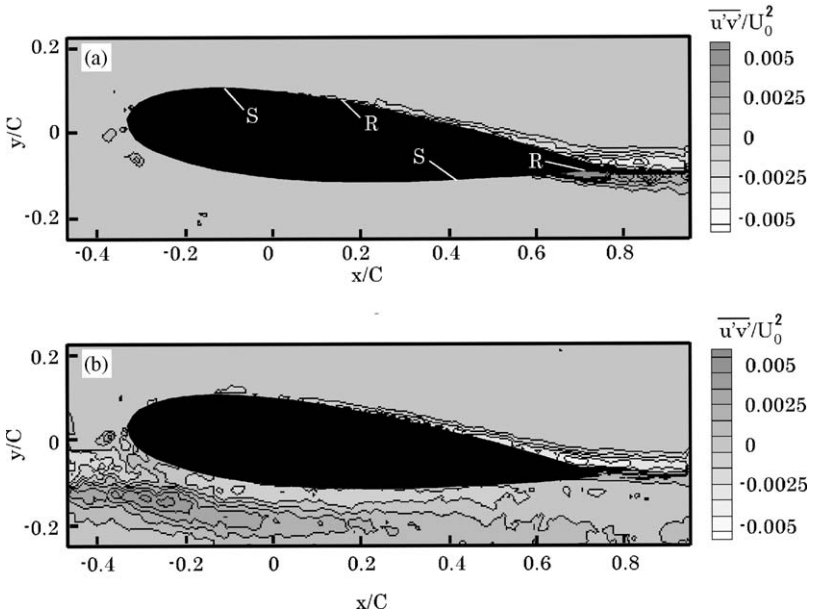


Fig. 14. Contour of Reynolds stress around airfoil at $\alpha = 6^\circ$ (R, reattachment; S, separation). (a) without cylinder and (b) with cylinder.

## 4. Conclusion

The influence of cylinder wake on tonal noise and aerodynamic characteristics of NACA0018 airfoil are studied experimentally in a uniform flow at a moderate Reynolds number. Measurements are taken on sound pressure level and spectrum, separation and reattachment points, pressure distribution, fluid forces and mean flow and turbulence characteristics around the airfoil with and without the cylinder wake. The tonal noise from the airfoil is suppressed by the influence of the cylinder wake, when it is placed on the pressure side of the airfoil. An improvement in the aerodynamic characteristics is also observed in the measurement with cylinder. They are caused by the removal of flow separation on the airfoil surface by influence of the cylinder wake, which is due to the wake-induced transition of the boundary layers from laminar to turbulent. The PIV measurements of the flow around the airfoil with the cylinder indicate that highly turbulent velocity fluctuation from the cylinder wake promotes the transition of the boundary layers on the airfoil and results in the formation of an attached turbulent boundary layer on the whole pressure surface of the airfoil. Such change of flow pattern on the pressure surface of the airfoil removes the periodic flow phenomena near the trailing edge of the airfoil and the following formation of vortex street in the downstream of the airfoil, which result in the suppression of tonal noise by the influence of the cylinder wake. The change in noise is due primarily to the pressure surface boundary layer, while the change in lift and drag is due primarily to the suction surface boundary layer.

## Acknowledgment

The authors would like to acknowledge the helpful suggestion by Prof. K. Nagaya from Gunma University.

## References

[1] R.W. Paterson, P.G. Vogt, M.R. Fink, C.L. Munch, Vortex noise of isolated airfoils, *Journal of Aircraft* 10 (1973) 296–302.
[2] C.K.W. Tam, Discrete tones of isolated airfoils, *Journal of Acoustical Society of America* 55 (1974) 1173–1177.
[3] H. Arbey, J. Bataille, Noise generated by airfoil profiles placed in a uniform laminar flow, *Journal of Fluid Mechanics* 134 (1983) 33–47.

[4] S. Akishita, Tone-like noise from an isolated two dimensional airfoil, AIAA paper, 1986, 86-1947.
[5] S.E. Wright, The acoustic spectrum of axial flow machines, *Journal of Sound and Vibration* 45 (1976) 165–223.
[6] R.E. Longhouse, Vortex shedding of low tip speed axial flow fans, *Journal of Sound and Vibration* 53 (1977) 25–46.
[7] E.C. Nash, M.V. Lowson, A. McAlpine, Boundary layer instability noise on airfoils, *Journal of Fluid Mechanics* 382 (1999) 27–61.
[8] A. McAlpine, E.C. Nash, M.V. Lowson, On the generation of discrete frequency tones by the flow around an airfoil, *Journal of Sound and Vibration* 222 (1999) 753–779.
[9] S. Tomimatsu, N. Fujisawa, Measurement of aerodynamic noise and unsteady flow field around a symmetrical airfoil, *Journal of Visualization* 5 (2002) 381–388.
[10] T. Nakano, H.-J. Kim, S. Lee, N. Fujisawa, Y. Takagi, A study on discrete frequency noise from a symmetrical airfoil in a uniform flow, *Proceedings of the 5th JSME-KSME Fluids Engineering Conference*, Nagoya, 2002, Pa.OS6-2-4.
[11] H. Pfeil, R. Herbst, T. Schroeder, Investigation of the laminar-turbulent transition of boundary layers disturbed by wakes, *ASME Journal of Engineering for Power* 105 (1983) 130–137.
[12] X. Liu, W. Rodi, Experiments on transitional boundary layers with wake induced unsteadiness, *Journal of Fluid Mechanics* 231 (1991) 229–256.
[13] N.K. Kriakides, E.G. Kastrinakis, S.G. Nychas, A. Goulas, Aspects of flow structure during a cylinder wake-induced laminar/turbulent transition, *AIAA Journal* 37 (1999) 1197–1205.
[14] R. Mailach, K. Vogeler, Wake-induced boundary layer transition in a low-speed axial compressor, *Flow, Turbulence and Combustion* 69 (2002) 271–294.
[15] D.C. Reda, M.C. Wilder, D.J. Farina, G. Zilliac, New methodology for the measurement of surface shear stress vector distributions, *AIAA Journal* 35 (1997) 608–614.
[16] N. Fujisawa, S. Shibuya, A. Nashimoto, T. Takano, Aerodynamic noise and flow visualization around two-dimensional airfoil, *Journal of Visualization Society of Japan* 21 (2001) 123–129 (in Japanese).
[17] N. Fujisawa, A. Aoyama, S. Kosaka, Measurement of shear-stress distribution over a surface by liquid-crystal coating, *Measurement Science and Technology* 14 (2003) 1655–1661.
[18] S. Zhong, Detection of flow separation and reattachment using shear-sensitive liquid crystals, *Experiments in Fluids* 32 (2002) 667–673.
[19] J. Kompenhans, M. Raffel, L. Dieterle, T. Dewhirst, H. Vollmers, K. Ehrenfried, C. Willert, K. Pengel, C. Kaehler, A. Schroeder, O. Ronneberger, Particle image velocimetry in aerodynamics, technology and applications in wind tunnels, *Journal of Visualization* 2 (2000) 229–244.
[20] N. Fujisawa, Y. Takizawa, A study on feedback control of edge tone by simultaneous flow visualization control and PIV measurement, *Measurement Science and Technology* 14 (2003) 1412–1419.
[21] N. Fujisawa, Y. Hashizume, Uncertainty analysis of temperature and velocity measured by liquid crystal visualization technique, *Measurement Science and Technology* 12 (2001) 1235–1242.
[22] R.D. Blevins, *Flow-Induced Vibration*, second ed, Van Nostrand Reinhold, New York, 1990 pp. 47–54.